Non-coding RNA Research 13 (2025) 43–56

Contents lists available at ScienceDirect

Non-coding RNA Research

journal homepage: www.keaipublishing.com/en/journals/non-coding-rna-research

Original Research Article

HNRNPC stabilizes m6A-modified AC145207.5 to accelerate tumorigenesis in colorectal cancer by impeding the Nrf2/GPX4 axis-mediated ferroptosis

Dan Liu [a,1], Shanshan Lin [a,1], Yueben Hu [b,1], Jianyong Xiong [c], Hongtao Wan [c], Yanglin Chen [c], Taohui Ding [c], Hu Zhao [c], Renjie Jiang [c], Zhijiang Huang [c], Dengke Yao [c], Ming Li [d], Xiaojian Zhu [c,*], Bo Yi [c,**]

[a] School of Pharmacy, Jiangxi Medical College, Nanchang University, Nanchang, 330006, PR China
[b] Department of Pharmacy, Nanchang People's Hospital, 330009, PR China
[c] 2nd Abdominal Surgery Department, Jiangxi Cancer Hospital, The Second Affiliated Hospital of Nanchang Medical College, Nanchang, Jiangxi, 330029, PR China
[d] Jiangxi Key Laboratory of Translational Cancer Research, Jiangxi Cancer Hospital, The Second Affiliated Hospital of Nanchang Medical College, Nanchang, Jiangxi, 330029, PR China

ARTICLE INFO

Keywords:
m6A
RNA binding protein
Ferroptosis
Nrf2/GPX4 signaling pathway

ABSTRACT

Ferroptosis is an apoptosis-independent cell death pathway characterized by heightened lipid peroxidation, which shows promise for tumor suppression. Despite extensive research on long non-coding RNAs (LncRNAs) in ferroptosis, their role in colorectal cancer (CRC) remains underexplored. We investigated the upregulation of AC145207.5 and HNRNPC expression in CRC tissues through public dataset analysis and in-house validation, identifying them as having significant diagnostic potential. *In vitro* experiments including MTS assay, transwell, and colony formation, alongside *in vivo* studies using xenograft models, elucidated the synergistic carcinogenic role of the HNRNPC/AC145207.5 axis in promoting the malignant characteristics of CRC. Mechanistically, the m6A reader HNRNPC stabilized m6A-modified AC145207.5, contributing to its stabilization and upregulation. Consequently, AC145207.5 activated the Nrf2/GPX4 axis, resulting in increased GPX4 expression, inhibition of GPX4-mediated ferroptosis, and facilitation of CRC progression. Our findings underscore the clinical relevance of the HNRNPC/AC145207.5 axis in CRC and illuminate its regulatory role in ferroptosis, suggesting implications for targeted precision medicine in CRC.

1. Introduction

Colorectal cancer (CRC) is a heterogeneous disease characterized by the uncontrolled growth of abnormal cells in the colon or rectum, presenting a clinical challenge in the realm of tumor prevention and treatment [1]. In 2023, CRC ranked as the second most frequently diagnosed cancer and the fifth leading cause of cancer-related deaths worldwide [2]. Given these findings, it is imperative to investigate novel biomarkers in CRC to enhance our understanding of molecular subtypes and facilitate the development of more effective diagnostic and therapeutic approaches.

Long non-coding RNAs (LncRNAs) are characterized by extensive nucleotide sequences exceeding 200 base pairs and lack protein-coding capacity [3]. Growing evidence underscores the involvement of diverse regulatory mechanisms, including dysregulated expression and mutations of LncRNAs, in the pathogenesis of CRC [4–6]. Notably, elevated levels of LncRNA AC145207.5 have been observed in CRC specimens compared to normal tissue. Prognostic analysis for AC145207.5 suggests its potential as a discerning biomarker for CRC diagnosis. However, its precise role in CRC remains unverified, warranting further exploration of its clinical functions.

N^6-methyladenosine (m6A) is the most prevalent internal RNA modification in mammalian cells, showcasing diverse functional implications associated with methylated RNAs that are recognized by m6A readers [7,8]. To investigate the putative RNA-binding proteins (RBPs) ssociated with AC145207.5, we leveraged public databases and

Peer review under the responsibility of Editorial Board of Non-coding RNA Research.
* Corresponding author.
** Corresponding author.
E-mail addresses: zhuxj8@mail2.sysu.edu.cn (X. Zhu), yibo@ncmc.edu.cn (B. Yi).
[1] These authors contributed equally to this work.

https://doi.org/10.1016/j.ncrna.2025.04.002
Received 19 August 2024; Received in revised form 26 March 2025; Accepted 6 April 2025
Available online 7 April 2025

identified significant interactions with HNRNPC, which is renowned for its roles as both m6A methyltransferase and an RBP. As a member of the HNRNP family, HNRNPC typically operates as an m6A reader, influencing various aspects of target RNA, including stability and degradation [9,10]. These actions impact the expression of target genes and modulate biological processes [11,12]. Notably, the precise mechanisms underlying the m6A reader HNRNPC's facilitation LncRNA stabilization during CRC tumorigenesis remain incompletely understood.

The accumulation of cytotoxic lipid peroxides on cellular membranes during ferroptosis plays a pivotal role in the regulation of cell death [13,14]. Recent studies have increasingly underscored the intimate relationship between ferroptosis and various facets of cancer, including its initiation and progression [15]. This burgeoning field of investigation has shed light on the intricate interplay between ferroptosis and cancer biology, with LncRNAs emerging as prominent regulators [16,17]. Our research findings have revealed that the depletion of AC145207.5 mitigates ferroptosis-related traits. Nevertheless, the precise mechanism through which AC145207.5 modulates ferroptosis in CRC remains inadequately elucidated, necessitating further exploration.

In our study, we unveiled a novel LncRNA, AC145207.5, which exhibits heightened expression levels in CRC tissues, and thus holds promise as a potential diagnostic marker. The upregulation of AC145207.5 is attributed to m6A modification and the subsequent binding by HNRNPC, resulting in the stabilization of AC145207.5. Our *in vitro* and *in vivo* investigations illustrate the role of AC145207.5 in promoting cell proliferation and invasion in CRC cells. Mechanistic analysis has uncovered that AC145207.5 activates the Nrf2/GPX4 pathway, a pivotal regulator of ferroptosis. Notably, the AC145207.5-activated Nrf2/GPX4 axis impedes ferroptosis and fosters the malignant phenotype of CRC. This study offers crucial insights into the mechanisms by which HNRNPC stabilizes AC145207.5 through m6A epigenetic modification, governing ferroptosis and its implications in CRC tumorigenesis.

2. Materials and methods

2.1. Study cohort and design

A total of 54 cases were randomly selected for inclusion in this study, which involved the collection of CRC specimens and non-tumorous tissues. The cases were selected between October 2020 and February 2023. All specimens were obtained from patients at Jiangxi Cancer Hospital who underwent surgical resection for CRC. Prior to use, all samples were immediately preserved in liquid nitrogen and stored at −80 °C. The study was approved by the Ethics Committee of Jiangxi Cancer Hospital (*No.*2022ky296). Written informed consent was obtained from all patients participating in the study.

2.2. Cell culture and cell line construction

The cell bank of the Chinese Academy of Sciences in Shanghai provided the SW480 (RRID: CVCL_0546) and HCT116 (RRID: CVCL_0291) human CRC cell lines. Dulbecco's Modified Eagle's Medium (DMEM; Gibco, #11965092) medium was employed for the cultivation of SW480 cells, while Roswell Park Memorial Institute 1640 (RPMI 1640; Gibco, # 11875119) medium was supplemented with 10% fetal bovine serum (FBS; Gibco, #10099-141), 100 U/mL penicillin and 100 μg/mL streptomycin for HCT116 cells. The cell cultures were maintained at 37°C with 5% CO_2 in a humidified environment.

The transfection of CRC cells with the target gene was conducted using an Oligofectamine™ transfection reagent (Thermo Fisher, #12252011). Subsequently, the transfected cells were harvested 48 h later. The specific shRNA sequences used in the transfection process are detailed in Table S1.

2.3. Real-time quantitative PCR (RT-qPCR)

Total RNA was extracted from CRC tissues and cell lines using Trizol reagent (#15596026) following the manufacturer's instructions. Reverse transcription was performed using the TB Green real-time PCR kit (Takara, Japan, #RR820A) to determine mRNA expression levels, with three replicates per measurement. All primers were obtained from Guangzhou RibBio Biotechnology Co., Ltd. (RibBio, Guangzhou, China). Table S2 provides a list of primers for RT-qPCR amplification.

2.4. Western blotting

Following transfection, cell lysates were prepared using RIPA lysis buffer and PMSF (Thermo Scientific, #36978, 100:1). The total protein content of the lysates was quantified using the BCA Protein Assay Kit (Beyotime Biotechnology, #P0012S) and subsequently boiled for 10 min at 100°C. The protein extracts were then fractionated by 10% SDS-PAGE (Solarbio, #P1200-50T) and transferred to PVDF membranes (Thermo Scientific, #88518). After blocking with 5% defatted milk, the membranes were incubated overnight at 4°C with the primary antibodies, followed by a 2-h incubation at room temperature with the secondary antibodies. The enhanced chemiluminescence (ECL; Solarbio, #PE0020) method was used for detection, and the data were analyzed using ImageJ software.

2.5. Cell proliferation assay

To assess cell viability, the MTS assay (Promega Biotech, #G5421) was utilized. 6-well plates (Thermo Scientific, #140675) were seeded with 500 cells per well and transfected with appropriate constructs for HCT116 and SW480 cells. Following the manufacturer's instructions, relative cell viability was determined. For colony formation assays, cells were plated onto six-well plates containing 10% fetal bovine serum (FBS). The cells were cultured, and media were replenished every 5 days. After two weeks of growth, the cells were fixed in 4% paraformaldehyde (Thermo Scientific, #FB002) for 30 min and stained with 0.1% crystal violet (Thermo Scientific, #R40052) before manual counting.

2.6. Wound healing assay

An *in vitro* wound healing assay was conducted to evaluate the migratory capacity of SW480 and HCT116 cells. The cells were seeded in six-well plates and allowed to form a confluent monolayer. Subsequently, a scratch was carefully created using a 20 μL pipettor (Rainin, USA). The scratch wounds were then imaged at 0 and 48 h using a microscope, and ImageJ software was utilized for the quantitative analysis of the relative wound size at each time point.

2.7. Transwell assay

For the cell invasion assay, a 24-well transwell insert chamber (Thermo Scientific, #142485) was utilized. Cells were treated, suspended in a serum-free culture medium, and then plated in the upper chamber at a concentration of 2×10^4 cells per well. After 48 h, the cells on the upper surface of the membrane were removed, and the chamber was washed with PBS. Following fixation with 4% paraformaldehyde, the cells were stained for 30 min with 0.1% crystal violet solution was performed, followed by rinsing with distilled water. Subsequently, cells that invaded from five randomly chosen fields were selected and quantified using ImageJ with the aid of a microscope.

2.8. Reactive oxygen species (ROS) staining assay

The levels of ROS were evaluated using a ROS Fluorometric Assay Kit (Invitrogen, #EEA019) according to the manufacturer's guidelines. The

cells were treated with a final concentration of 10 μM dihydroethidium (DHE) in a serum-free medium at 37°C for 15 min. Following this, the fluorescence intensity was quantified to determine the cellular ROS levels.

2.9. Malondialdehyde (MDA) assay

To quantify the levels of MDA in cellular samples, the Cell MDA Colorimetric Assay Kit (Invitrogen, #EEA015) was employed. This assay kit utilizes the reaction between MDA and thiobarbituric acid (TBA). Following treatment, CRC cells were collected, lysed, and sonicated. The lysates were then quantified, and the MDA working solution was added. The MDA content was determined by measuring the absorbance at 532 nm using a microplate reader.

2.10. Iron assay

The concentration of Fe^{2+} was determined using an iron assay kit (Biovision, #MA-0103). Following cell lysis and centrifugation, protein quantification was conducted, and the resulting supernatant was used to determine the iron ion concentration. Blank control tubes, standard quality control tubes, and sample tubes were prepared according to the provided guidelines. The samples were incubated in a water bath at 60°C for 1 h. Subsequently, the reagent for iron ion detection was thoroughly mixed and incubated at room temperature for 30 min. Absorbance was measured at a wavelength of 593 nm.

2.11. Glutathione (GSH) and glutathione oxidized (GSSG) assays

The GSH and GSSG levels were assessed using the GSH and GSSG Colorimetric Assay Kit (Invitrogen, #EEA020). This assay kit employs a colorimetric method in which the formation of a yellow product (5-thio-2-nitrobenzoic acid) occurs. The GSH content can be indirectly quantified by measuring the optical density (OD) at 450 nm.

2.12. Fluorescence in situ hybridization (FISH)

The subcellular localization of AC145207.5 was examined using the FISH Tag™ RNA Multicolor Kit (Invitrogen, #F32956). Following fixation of the cells with 4% formaldehyde, permeabilization was performed using pre-chilled permeabilization solutions, and subsequent blocking was carried out with a pre-hybridization solution provided in the kit. The cells were then subjected to hybridization with the AC145207.5 FISH probe mixture at 37°C overnight. Following three washes, DAPI was employed for nuclear staining, and the cells were ultimately affixed to slides using a mounting medium. Subsequently, stained cells were visualized using a confocal laser scanning microscope (Carl Zeiss Microimaging) to capture images.

2.13. RNA stability assay

To assess RNA stability, cells were exposed to 5 μg/mL actinomycin D (Sigma, #A9415). HCT116 or SW480 cells were transfected with either sh-*NC* or sh-*HNRNPC*. Subsequently, total RNA was extracted at 0, 3, and 6 h post-treatment with actinomycin D for qPCR analysis.

2.14. RNA Immunoprecipitation (RIP) and Methylated RNA Immunoprecipitation (Me-RIP) qPCR assays

Following the aforementioned protocol, RIP experiments were performed. Specifically, cell extracts were co-immunoprecipitated using HNRNPC (ZEN-BIOSCIENCE, #R381235, 1:50) and m6A (CST, #56593S, 1:5000) antibodies. The Magna RIP™ RNA-Binding Protein Immunoprecipitation Kit (Millipore, #17–701) was employed for conducting the RIP experiments. Subsequently, the RNA recovered from the immunoprecipitation was analyzed using qPCR to quantify specific RNA targets.

2.15. Immunohistochemistry (IHC) staining

The tissue slides underwent rehydration in graded alcohol solutions and were rinsed with distilled water after being deparaffinized in xylene. Following this, the slides were incubated overnight at 4°C with primary antibodies specific for HNRNPC (ZEN-BIOSCIENCE, #R381235, 1:200), Nrf2 (Abcam, #ab137550, 1:500), GPX4 (Abcam, #ab125066, 1:100), and Ki-67 (Proteintech, #27309-1-AP, 1:5000). Subsequently, secondary antibodies, including HRP-conjugated goat anti-rabbit IgG (Proteintech, #PR30011, 1:5000) and HRP-conjugated goat anti-rabbit IgG (BOSTER, #BA1050, 1:5000), were applied using the conventional avidin-biotin peroxidase complex method for 1 h at room temperature. Counterstaining was then performed using hematoxylin, followed by dehydration and mounting of the slides. Protein expression levels were further analyzed using an Olympus BX53 microscope.

2.16. Animal in vivo experiments

The CRC cell line HCT116 were cultured in DMEM medium supplemented with 10% FBS. After trypsin digestion, the cells were combined with 50% Matrigel (BD, #354234) to achieve a final concentration of 5×10^6 cells/200 μL. To establish a xenograft mouse model of CRC, commonly known as a cell-derived xenograft (CDX) model, a cell suspension from HCT116 was subcutaneously injected into the axillary region of ten five-week-old BALB/c Nude mice. These mice were procured from SJA Laboratory Animal Co., Ltd. (Hunan, China) and were acclimated to specific pathogen-free (SPF) conditions for one week prior to the experiment. The animal experimentation in this study was conducted in compliance with ethical standards and received approval from the Ethics Committee of Jiangxi Cancer Hospital (*No*.2023.053), adhering to institutional guidelines and regulations. Tumor size and volume were monitored until the conclusion of the experimental tumor harvesting period, after which the tumors were surgically excised for subsequent analysis and research purposes.

2.17. Statistical analysis

All values were presented as means ± standard deviation (SD), and statistical analyses and visualization were performed using GraphPad Prism 7 (GraphPad Prism, RRID: SCR_002798). The significance of differences between groups was assessed using one-way ANOVA and Student's paired or unpaired t-tests. The experiments were conducted as independent biological replicates and repeated at least three times. Results were labeled as follows: ns indicates not significant.

3. Results

3.1. The HNRNPC/AC145207.5 axis functions synergistically to promote the adverse progression of CRC

Tumor heterogeneity represents a hallmark feature of malignant tumors and holds substantial clinical relevance for the efficacy of treatment [18,19]. To gain insight into the critical regulatory factors during the malignant progression of CRC, we conducted comprehensive transcriptomic analyses, comparing samples from normal (n = 51) and tumor (n = 647) tissues sourced from TCGA. The data revealed that AC145207.5 was significantly upregulated in CRC tissues (TOP 1, Fold Change = 4.073, $P < 0.0001$) (Fig. 1a). To gain a comprehensive understanding of AC145207.5 expression patterns in CRC, we meticulously analyzed its post-transcriptional levels using data from TCGA databases. Our results showed a marked upregulation of AC145207.5 expression in CRC tissues compared with paraneoplastic tissues (Fig. 1b). To corroborate these observations, we performed RT-qPCR on 47 to 50 post-operative clinical samples obtained from Jiangxi Cancer Hospital.

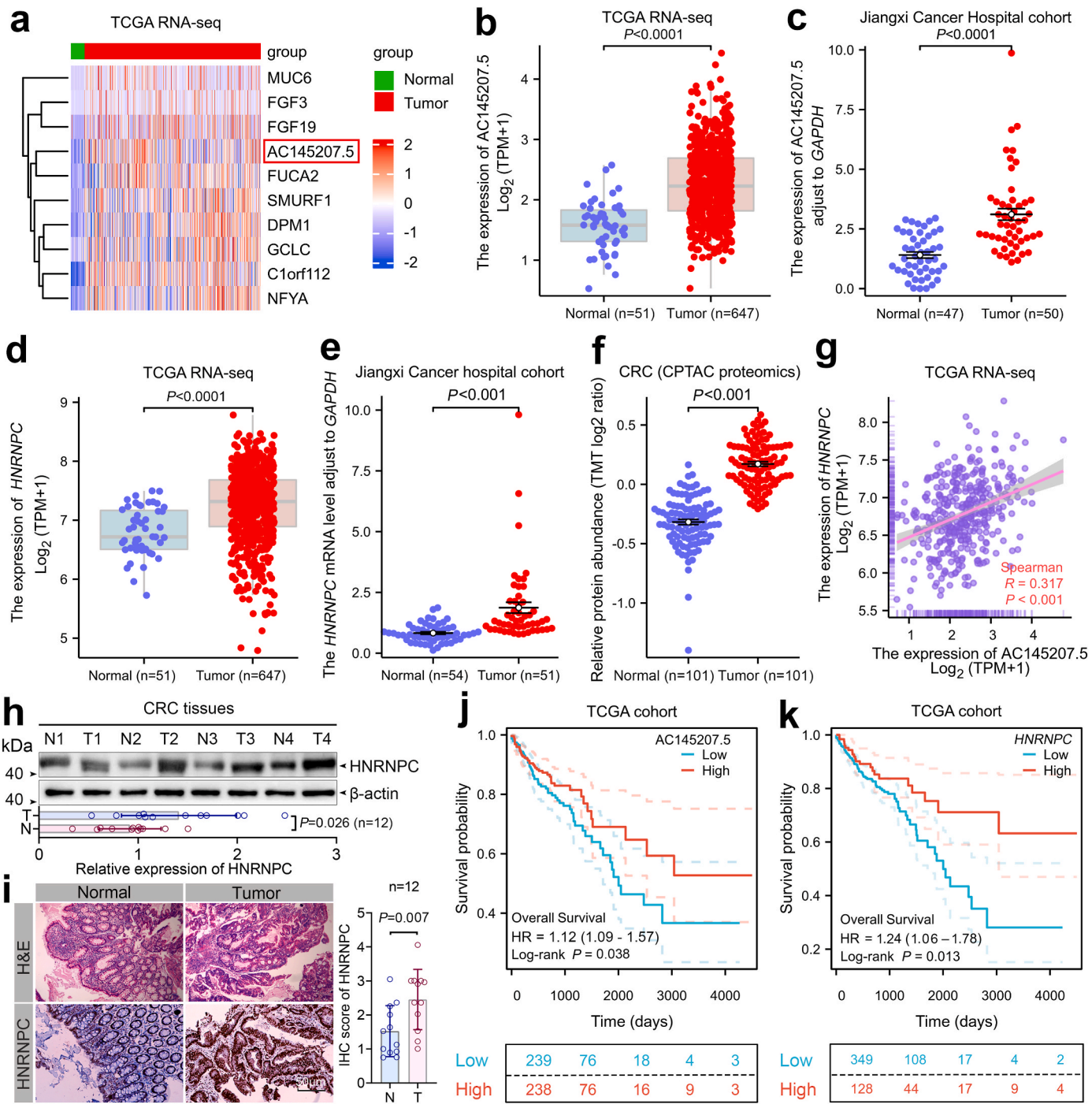

Fig. 1. The HNRNPC/AC145207.5 axis functions synergistically to promote the adverse progression of CRC. (**a**) Heat map analysis of differentially expressed genes (DEGs) in CRC tissues compared to normal tissues using the TCGA database. (**b**) Analysis of AC145207.5 expression in CRC tissues compared with normal tissues using TCGA database. (**c**) RT-qPCR analysis of AC145207.5 expression in CRC tissues compared with adjacent normal tissues. (**d**) Analysis of *HNRNPC*-mRNA expression in CRC tissues compared with normal tissues using TCGA database. (**e**) RT-qPCR analysis of *HNRNPC*-mRNA expression in CRC tissues compared with adjacent normal tissues. (**f**) Analysis of HNRNPC protein expression in CRC tissues compared with normal tissues using CPTAC database. (**g**) Feature plots depict the correlation between AC145207.5 and *HNRNPC* in the TCGA-CRC RNA-seq (n = 641). (**h**) Western blotting analysis of HNRNPC protein expression in CRC tissues and their corresponding normal tissues. β-actin is used as a loading control. (**i**) Representative images of HNRNPC expression in paired CRC tissue versus normal samples from the Jingxi Cancer Hospital cohort using IHC staining. (**j and k**) Kaplan-Meier analysis of overall survival in two groups of CRC patients stratified by high and low expression of AC145207.5 (i) and *HNRNPC* (j) using the data from the TCGA database. Each bar represents the mean values ± SD. All statistical analyses were performed using the Mann-Whitney *U* test.

Consistently, the AC145207.5 expression was significantly elevated in CRC tissues compared with their corresponding adjacent normal tissues (Fig. 1c).

To unravel the underlying factors responsible for the significant upregulation of AC145207.5 in CRC, we utilized the ENCORI database to predict RBPs associated with AC145207.5. Our analysis uncovered significant interactions between AC145207.5 and FMR1, ELAVL1, HNRNPC, and IGFBP2, which function as m6A methyltransferases and

RBPs (Fig. S1a). Similarly, AC145207.5 was also found to be significantly positively correlated with *ELAVL1*, *HNRNPC*, and *ILF3* expression at the transcriptional level (Fig. S1b). To validate our findings, we proceeded to knock down *FMR1*, *ELAVL1*, *HNRNPC*, and *IGFBP2*, which resulted in a subsequent decrease in AC145207.5 expression in HCT116 cells with *HNRNPC* knocked down (Fig. S1b). However, knockdown of *FMR1*, *ELAVL1*, and *IGFBP2* had no significant effect on AC145207.5 expression (Fig. S1c–e).

Based on the above findings, it is plausible to speculate that HNRNPC, as a reader protein of m6A modifications, potentially exerts

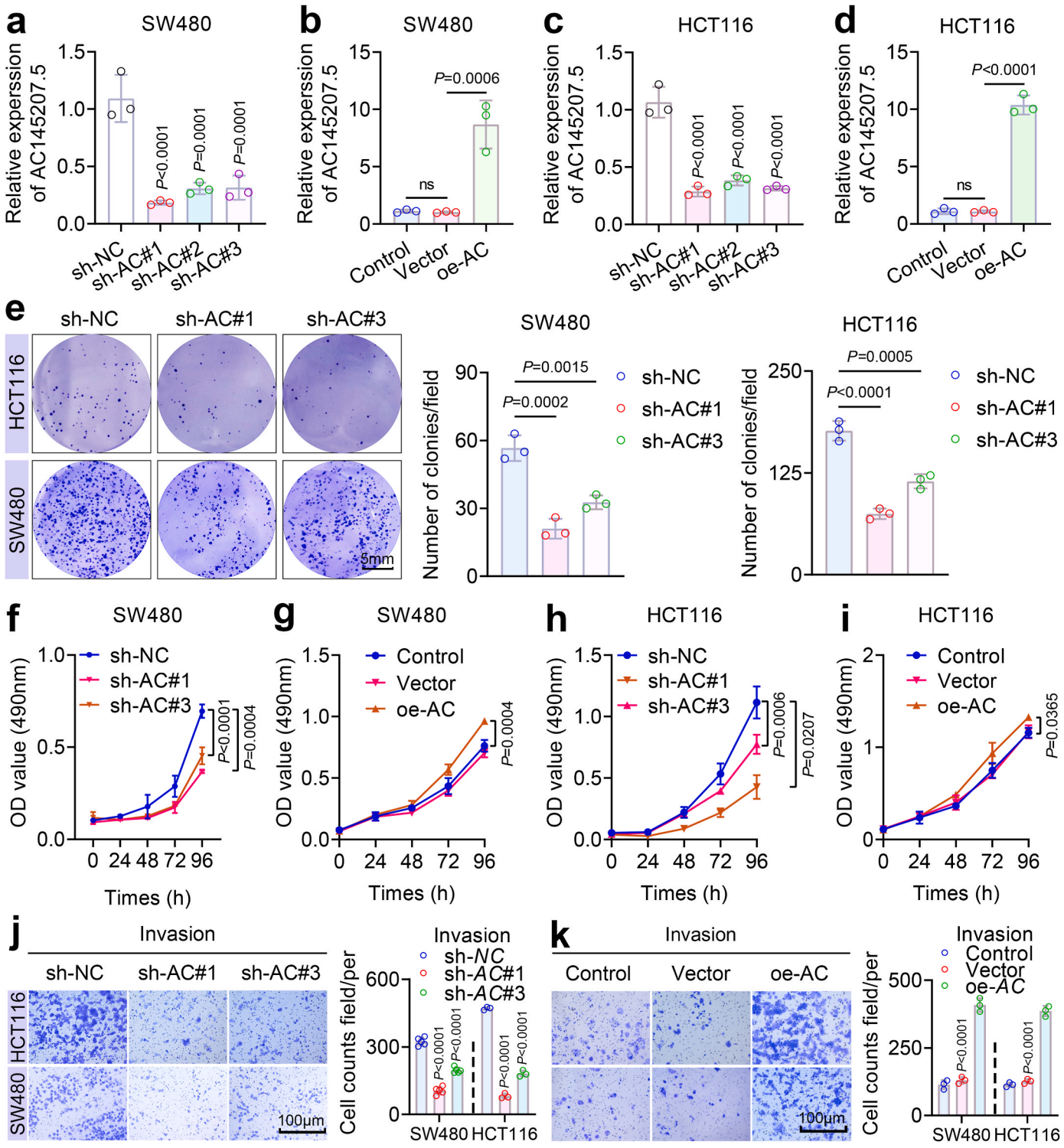

Fig. 2. AC145207.5 induces tumorigenesis and promotes tumor progression in CRC. (**a-d**) RT-qPCR analyses of changes in AC145207.5 expression levels in SW480, and HCT116 following knockdown or overexpression of AC145207.5. (**e**) Colony formation assay showing the effect of AC145207.5 on survival potential in CRC cell lines. (**f-i**) MTS assay demonstrating the impact of AC145207.5 knockdown or overexpression on cell viability in SW480 and HCT116 cell lines. (**j and k**) Transwell assays were employed to assess the impact of AC145207.5 knockdown (j) or overexpression (k) on the invasive capabilities of HCT116 and SW480 cells. Each bar represents the mean values ± SD.

influence on the degradation of AC145207.5, thereby augmenting RNA abundance and consequently stabilizing its expression. Our results also demonstrated a significant upregulation of *HNRNPC* expression in CRC tissues compared with paraneoplastic tissues (Fig. 1d). To further confirm these findings, RT-qPCR was performed on 54 to 51 post-operative clinical samples obtained from Jiangxi Cancer Hospital, showing significantly elevated *HNRNPC* expression in CRC tissues compared with their corresponding adjacent normal tissues (Fig. 1e).

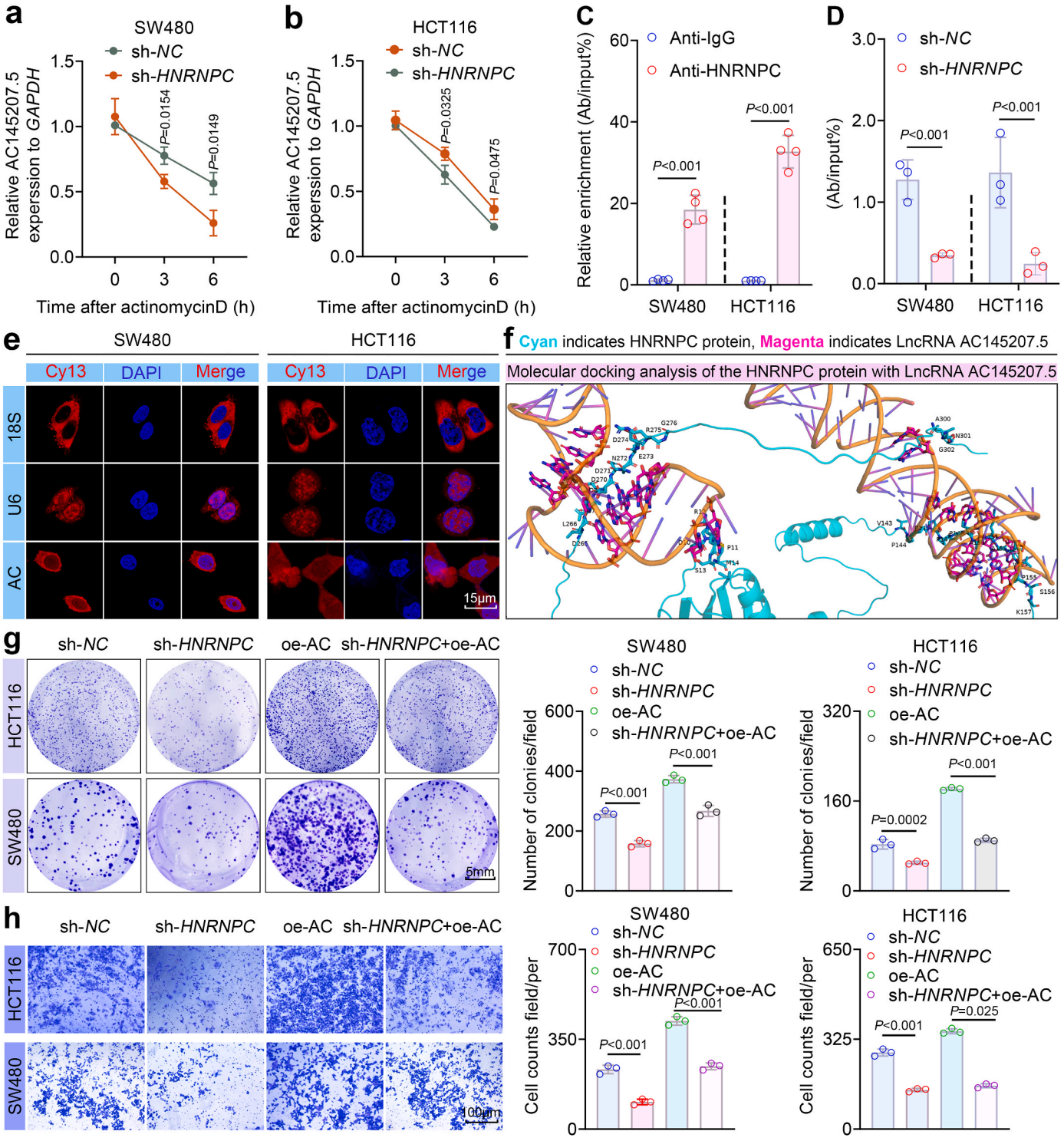

Fig. 3. HNRNPC mediates malignant behaviors by regulating m6A-modified AC145207.5 in CRC cells. (**a and b**) The half-life (t1/2) of AC145207.5 decay was reduced after down-regulating *HNRNPC* in SW480 (a) and HCT116 (b) cells. (**c**) RNA-RIP followed by qPCR showed binding of HNRNPC with AC145207.5 in SW480 and HCT116 cells. (**d**) RIP followed by qPCR showed binding of AC145207.5 with anti-m6A in SW480 and HCT116 cells after down-regulating HNRNPC. (**e**) FISH assay was performed to observe the localization of AC145207.5 in SW480 and HCT116 cells. (**f**) The top-ranked 3D docking conformation of AC145207.5 (AlphaFold3 predicts tertiary structure) and HNRNPC (AF-P07910-F1-model_v4) is shown using Pymol 3.0. (**g**) Rescue experiments assessing colony-forming abilities treated by co-transfected *HNRNPC* silencing and AC145207.5 overexpression in SW480 and HCT116 cells. (**h**) Rescue experiments detecting invasion abilities treated by co-transfected *HNRNPC* silencing and AC145207.5 overexpression in SW480 and HCT116 cells, assayed by transwell assays.

Additionally, data from the CPTAC database confirmed that HNRNPC protein expression was significantly upregulated in CRC tissues (Fig. 1f). Subsequent correlation analysis of transcript levels revealed a significant positive correlation between AC145207.5 expression and HNRNPC expression (Fig. 1g). Furthermore, IHC staining indicated significantly higher staining intensity and a greater proportion of HNRNPC-positive cells in paired CRC tissue samples compared with their corresponding normal tissues (Fig. 1i). This was further confirmed by Western blotting experiments (Fig. 1h). Moreover, our results suggest that AC145207.5 may hold promise as a clinically relevant tumor marker for the diagnosis and therapeutic monitoring of CRC, as indicated by survival analysis and ROC curve analysis (Fig. 1j and k). In light of these observations, we postulate that the HNRNPC/AC145207.5 axis may act synergistically to drive the malignant progression of CRC.

3.2. AC145207.5 potentiates proliferation and invasion of the malignant phenotype of CRC cells in vitro

To investigate the functional implications of AC145207.5 in CRC cells, we designed three specific shRNAs (shRNA#1, shRNA#2, and shRNA#3, abbreviated as sh-AC) and an overexpression plasmid (oe-AC145207.5, abbreviated as oe-AC) targeting AC145207.5. These molecular constructs were transfected into HCT116 and SW480 cells to modulate the expression levels of AC145207.5. The results obtained from RT-qPCR analysis demonstrated statistically significant alterations in AC145207.5 expression upon transfection with either the sh-AC or oe-AC constructs (Fig. 2a–d). Notably, shRNA#2 exhibited a comparatively diminished effect. Therefore, shRNA#1 and shRNA#3 were prioritized for subsequent experiments to suppress AC145207.5 expression.

Firstly, the colony formation assay revealed that the downregulation of AC145207.5 significantly impaired the ability of CRC cells to form colonies (Fig. 2e). Subsequent evaluation using the MTS assay at various time points (0, 24, 48, 72, and 96 h) demonstrated a marked decrease in cell viability following the knockdown of AC145207.5 in both HCT116 and SW480 cells (Fig. 2f and h). Conversely, overexpression of AC145207.5 led to enhanced cell viability (Fig. 2g and i). Furthermore, assessment of the invasive capabilities of CRC cells via transwell assays revealed a reduction in invasiveness upon interference with AC145207.5, contrasting with the augmented invasion observed upon overexpression of AC145207.5, as depicted in Fig. 2j and k. To summarize, our findings provide compelling evidence that heightened expression of AC145207.5 fosters the progression of a malignant phenotype in CRC cells.

3.3. HNRNPC facilitates the cancer cell biological phenotype by stabilizing the expression of m6A-modified AC145207.5

Drawing upon the enlightening results of our bioinformatics analysis, we uncovered a substantial correlation between HNRNPC and AC145207.5. Intrigued by this association, we embarked on a meticulous exploration to unravel the intricate interplay between HNRNPC, AC145207.5, and m6A methylation stability in the context of CRC progression. To this end, we conducted RNA stability assays to shed light on the dynamics of AC145207.5 in response to *HNRNPC* knockdown and treatment with actinomycin D at various time points. The captivating findings of these assays unveiled a striking reduction in the half-life of AC145207.5 within CRC cells upon *HNRNPC* knockdown (Fig. 3a). Furthermore, when treated with actinomycin D, a potent transcriptional inhibitor, the degradation of AC145207.5 was accelerated over a range of time points (Fig. 3b). These compelling results provide valuable insights into the intricate regulatory mechanisms governing the stability of AC145207.5, mediated by the interplay between HNRNPC and m6A methylation, thus contributing to a deeper understanding of CRC pathogenesis.

To establish the potential link between HNRNPC and AC145207.5, we initiated our investigation with RIP-qPCR assays. Remarkably, compared to the input control, we observed a significant enrichment of AC145207.5 in association with HNRNPC expression in HCT116 cells (Fig. 3c). Moreover, employing the Cuilab tool, we identified an m6A binding-qualified AGACU motif within AC145207.5, further strengthening the potential interaction between HNRNPC and AC145207.5 (Fig. S2a). Similarly, CLIP-seq analysis revealed AC145207.5 binding peaks on HNRNPC in several CRC cell lines, including HCT116, GP5D, and LoVo (Fig. S2b). Additionally, using Me-RIP assays, we successfully demonstrated that the m6A antibody was capable of effectively pulling down AC145207.5, while the depletion of *HNRNPC* significantly hindered the enrichment of AC145207.5 (Fig. 3d).

Considering the well-established nuclear localization of HNRNPC [20], we sought to determine the cellular distribution of AC145207.5 through fluorescence in situ hybridization. Strikingly, our results confirmed the presence of AC145207.5 in both the nucleus and cytoplasm of HCT116 and SW480 cells (Fig. 3e), suggesting a potential interaction between AC145207.5 and HNRNPC within the nucleus. Furthermore, molecular docking analysis of protein three-dimensional structures, revealed a stable interaction between AC145207.5 and HNRNPC protein (Fig. 3f).

To shed light on the regulatory mechanisms governed by HNRNPC and AC145207.5 in CRC cell characteristics, we conducted MTS assays (Fig. S3a and b) and Wound healing assays (Fig. S3c) to analyze the impact of *HNRNPC* downregulation on cell proliferation and invasion in HCT116 and SW480 cells. As anticipated, the downregulation of *HNRNPC* expression exerted a pronounced inhibitory effect on the proliferative and migratory capabilities of both cell lines. Additionally, transwell assays were employed to assess their invasive capabilities, revealing a significant reduction in the invasive potential of HCT116 and SW480 CRC cells upon downregulation of *HNRNPC* (Fig. S3d).

To further elucidate the tumor-promoting function of HNRNPC, rescue experiments were conducted, wherein the overexpression of AC1452075 successfully reversed the inhibition of tumor cell migration and invasion caused by *HNRNPC* knockdown (Fig. 3g and h). These compelling findings provide robust support for the hypothesis that HNRNPC promotes CRC cell proliferation and invasion by stabilizing AC145207.5 expression, unraveling a novel regulatory axis with significant implications in CRC pathogenesis.

3.4. AC145207.5 facilitates CRC progression by suppressing ferroptosis

To unravel the intricate web of downstream molecular targets influenced by AC145207.5 in CRC, we conducted a comprehensive RNA-seq analysis on HCT116 cells engineered with lentiviral vectors carrying sh-AC. This approach unveiled a noteworthy differential expression in 5705 genes, highlighting the profound impact of AC145207.5 on cellular processes. Subsequent GO analysis unmasked their involvement in a myriad of biological regulatory pathways, including cholesterol and fatty acid metabolism, as well as carbohydrate metabolism, among others (Fig. 4a). Moreover, KEGG analysis identified a striking enrichment in diverse signaling pathways, with a particular emphasis on the pivotal role of Ferroptosis (Fig. 4b). These enrichments underscore the significance of ferroptosis in orchestrating the biological functions modulated by AC145207.5, offering a deeper understanding of its molecular mechanisms in CRC.

To validate the intriguing hypothesis, our initial investigations unveiled compelling evidence indicating that the decline in AC145207.5 expression led to a remarkable surge in ROS production. Conversely, the overexpression of AC145207.5 exhibited a potent inhibitory effect on ROS production within CRC cells (Fig. 4c). Intriguingly, knockdown of AC145207.5 expression resulted in a significant elevation in cellular Fe^{2+} concentration, while overexpression led to a notable reduction in cellular Fe^{2+} concentration (Fig. 4d). To further substantiate our findings, we administered the ferroptosis inhibitor Fer-1 and observed its remarkable efficacy in abolishing the CRC cell death induced by AC145207.5 downregulation, consequently enhancing cell viability

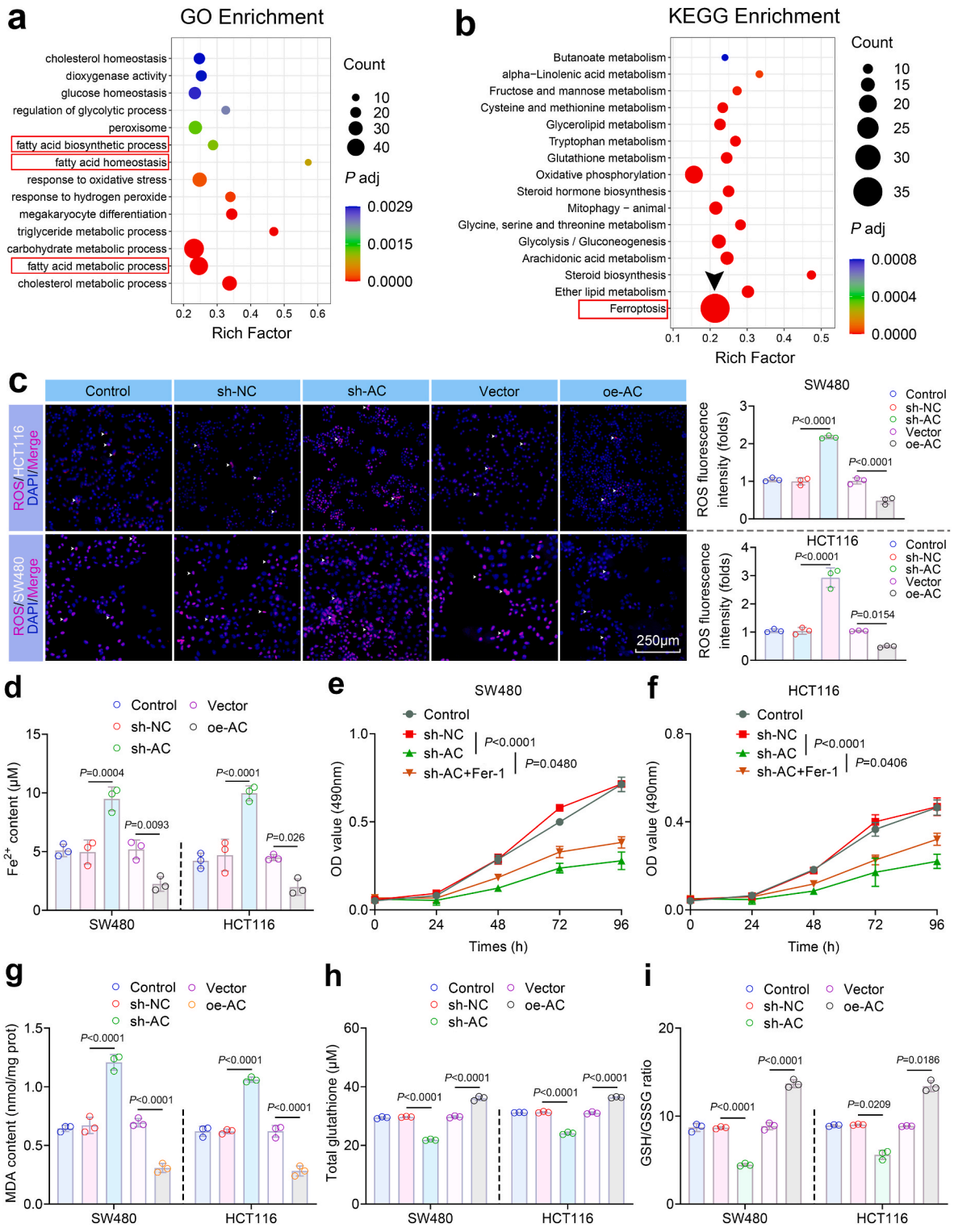

Fig. 4. AC145207.5 enhances CRC cell proliferation through ferroptosis activation. (**a**) GO enrichment analysis performed for AC145207.5 knockdown in HCT116 cells. (**b**) KEGG pathway enrichment analysis conducted for AC145207.5 knockdown in HCT116 cells. (**c**) Levels of ROS detected after AC145207.5 knockdown or overexpression in HCT116 and SW480 cells. (**d**) Intracellular Fe^{2+} concentration assayed after AC145207.5 knockdown or overexpression in HCT116 and SW480 cells. (**e and f**) Fer-1 (5 μM) reversed the decreased cell viability induced by AC145207.5 knockdown in HCT116 and SW480 cells. (**g**) MDA levels analyzed after AC145207.5 knockdown or overexpression in HCT116 and SW480 cells. (**h and i**) Total GSH levels and the ratio of reduced GSH/GSSG determined after AC145207.5 knockdown or overexpression in HCT116 and SW480 cells. Statistical analyses were performed using the one-way ANOVA.

(Fig. 4e–f). Collectively, these captivating findings provide compelling evidence that AC145207.5 suppresses ferroptosis in CRC cells, thereby promoting the malignant phenotype.

Ferroptosis, characterized by redox-active iron overload, reactive accumulation, lipid peroxidation, and GSH depletion, was meticulously examined through the measurement of intracellular chelate iron, ROS, MDA, GSH, and GSH/GSSG ratio. As anticipated, downregulation of AC145207.5 significantly amplified Fe^{2+}, ROS, and MDA levels, while

concurrently depleting total GSH and diminishing the GSH/GSSG ratio. Conversely, upregulation of AC145207.5 strikingly diminished Fe^{2+}, ROS, and MDA levels, while eliciting pronounced increases in total GSH and the GSH/GSSG ratio (Fig. 4g–i). These compelling findings unequivocally indicate that ferroptosis is the predominant mechanism by which the downregulation of AC145207.5 instigates cell death in CRC cells, unveiling a novel avenue for potential therapeutic interventions.

3.5. AC145207.5 attenuates ferroptosis via the Nrf2/GPX4 signaling pathway

To delve deeper into the specific mechanism by which AC145207.5 inhibits ferroptosis, we conducted transcriptome sequencing. The RNA-seq analysis revealed that downregulation of AC145207.5 in HCT116 resulted in the upregulation of 4176 genes and the downregulation of 1529 genes (Fig. 5a). Notably, the gene *GPX4* emerged as a prominent candidate warranting closer examination, given its pivotal role as a key regulator of ferroptosis (Fig. 5b). Nrf2, recognized as the master transcriptional regulator of antioxidant gene expression, holds significant importance in this context, with GPX4 being one of its downstream antioxidant enzymes. Building upon this intricate network, we hypothesized that the functional mechanism of AC145207.5 may be intricately intertwined with the Nrf2/GPX4 signaling axis.

To validate this hypothesis, Western blotting analysis was conducted, revealing that changes in AC145207.5 expression at the RNA level correspondingly influenced the levels of Nrf2 and GPX4 proteins (Fig. 5c). Additionally, IHC analysis unveiled heightened levels of Nrf2 and GPX4 expression in tumors characterized by elevated AC145207.5 expression (Fig. 5f). To explore the potential regulatory role of AC145207.5 in the Nrf2/GPX4 pathway and its implications for ferroptosis, we conducted rescue assays using specific activators (TBHQ) and inhibitors (ML385) of Nrf2 in cells with modulated AC145207.5 expression levels. Notably, alterations in AC145207.5 expression led to corresponding changes in GPX4 expression, with upregulation of AC145207.5 resulting in increased GPX4 expression, and downregulation leading to decreased GPX4 expression. However, the impact of AC145207.5 on GPX4 expression was partially reversed by the administration of TBHQ or ML385 (Fig. 5d and e). These results suggest that *GPX4* could potentially function as a downstream target in the AC145207.5/Nrf2 signaling pathway. Additionally, the pro-ferroptotic effect of downregulating AC145207.5 in CRC cells was counteracted by TBHQ, as evidenced by the elevated levels of MDA, total glutathione, and the GSH/GSSG ratio (Fig. 5g, i and k). Conversely, ML385 reversed the inhibitory effect on ferroptosis induced by AC145207.5 overexpression (Fig. 5h, j and k).

To further investigate whether *GPX4* is a critical downstream gene of AC145207.5 in CRC, we designed *GPX4* siRNAs and transfected them into CRC cells with elevated expression of AC145207.5. Our results demonstrated that AC145207.5 overexpression significantly increased MDA levels, total glutathione content, and the GSH/GSSG ratio. However, co-transfection of si-*GPX4* reversed these effects (Fig. 5m–o). These findings collectively provide compelling evidence suggesting that the Nrf2/GPX4 pathway mediates the regulatory effect of AC145207.5 on ferroptosis.

3.6. AC145207.5 knockdown suppressed tumorigenesis in CRC xenograft model

To elucidate the nuanced functions of AC145207.5 in CRC tumorigenesis *in vivo*, HCT116 cells with AC145207.5 knockdown were subcutaneously implanted into BALB/c nude mice and allowed to grow for approximately five weeks. Upon reaching the eighth day post-transplantation, discernible xenograft tumors had effectively formed. Remarkably, tumors originating from mice subjected to AC145207.5 knockdown exhibited substantially diminished size (Fig. 6a), reduced weight (Fig. 6c), and attenuated volume (Fig. 6d) compared to those in the sh-*NC* group. This disparity in tumor morphology was further validated through histological examination using H&E staining (Fig. 6b). IHC analysis of the xenograft tumors disclosed a conspicuous decrease in the expression levels of Ki-67, Nrf2, and GPX4 in the AC145207.5 knockdown cohort compared to the sh-*NC* group (Fig. 6e and f). Collectively, our *in vivo* investigations in mice underscored the pivotal role of AC145207.5 inhibition in impeding the proliferation of xenograft tumors, implicating its potential regulatory function in CRC progression. Moreover, our findings suggest that AC145207.5 may exert its regulatory influence on CRC development through modulation of ferroptosis via the Nrf2/GPX4 signaling pathway.

4. Discussion

The burgeoning body of recent research has brought into sharp focus the pivotal significance of LncRNAs in cellular development and the pathogenesis of various human diseases, particularly cancer [21,22]. Perturbations in LncRNA expression have been implicated in driving the unchecked proliferation and metastasis of malignant tumors [23]. Employing a multifaceted analytical approach encompassing biochemical, and cell biology methodologies, our study elucidates the oncogenic influence of AC145207.5 in CRC, impacting tumorigenesis and ferroptosis pathways. Through a series of meticulous experiments conducted both *in vitro* and *in vivo*, we consistently observe that the downregulation of AC145207.5 significantly impedes tumor cell proliferation and invasion by fostering ferroptosis in CRC. These compelling findings underscore the critical role of heightened AC145207.5 expression in orchestrating the malignant progression of CRC.

HNRNPC serves as an m6A reader, a prevalent RNA modification that significantly influences the abundance, stability, splicing, and transport of target RNAs [9]. Previous research has implicated HNRNPC in the malignant progression of various tumors [20,24]. However, the precise regulatory mechanisms through which m6A modification and its reader modulators contribute to tumorigenesis, particularly in the context of CRC, remain incompletely understood. Our study has unveiled a pivotal regulatory interplay between the m6A reader HNRNPC and modified AC145207.5 through m6A modulation patterns, playing a crucial role in GPX4-mediated ferroptosis during CRC tumorigenesis. Our findings demonstrate that heightened HNRNPC expression correlates with increased levels of AC145207.5, culminating in augmented cell proliferation via the stabilization of m6A-modified AC145207.5. Furthermore, elevated expression of HNRNPC and AC145207.5 in human CRC tissues was associated with a poorer prognosis.

Notably, our study has uncovered a significant association between AC145207.5 and HNRNPC, a key oncogenic m6A modulator, in terms of their impact on cellular characteristics in CRC [25]. This novel correlation holds substantial implications for the development of biomarkers and therapeutic targets for the diagnosis and monitoring of CRC treatment efficacy. While the functional role of HNRNPC in various cancers is well-established [26,27], the specific epigenetic regulatory network and functional role of AC145207.5 in CRC have yet to be fully elucidated. Our study provides groundbreaking evidence demonstrating that AC145207.5 functions as a novel target of HNRNPC, an m6A reader that stabilizes the expression of AC145207.5. The collaborative promotion of CRC cell proliferation and pathogenesis by AC145207.5 and HNRNPC offers valuable insights into the biology of CRC.

Ferroptosis, an emerging form of regulated cell death triggered by oxidative stress, has garnered attention for its potential contribution to tumor development, offering significant implications for cancer prevention and treatment [28,29]. Our study represents the first to explore the upregulation of AC145207.5 in CRC, elucidating its role in suppressing ferroptosis and promoting tumor growth. Through RNA-seq, we identified *GPX4* as a downstream target gene of AC145207.5, well-known for its involvement in ferroptosis [13,30]. Previous research has demonstrated that specific medications can reduce GPX4 protein levels by targeting the mTORC1 pathway, sensitizing cancer cells to

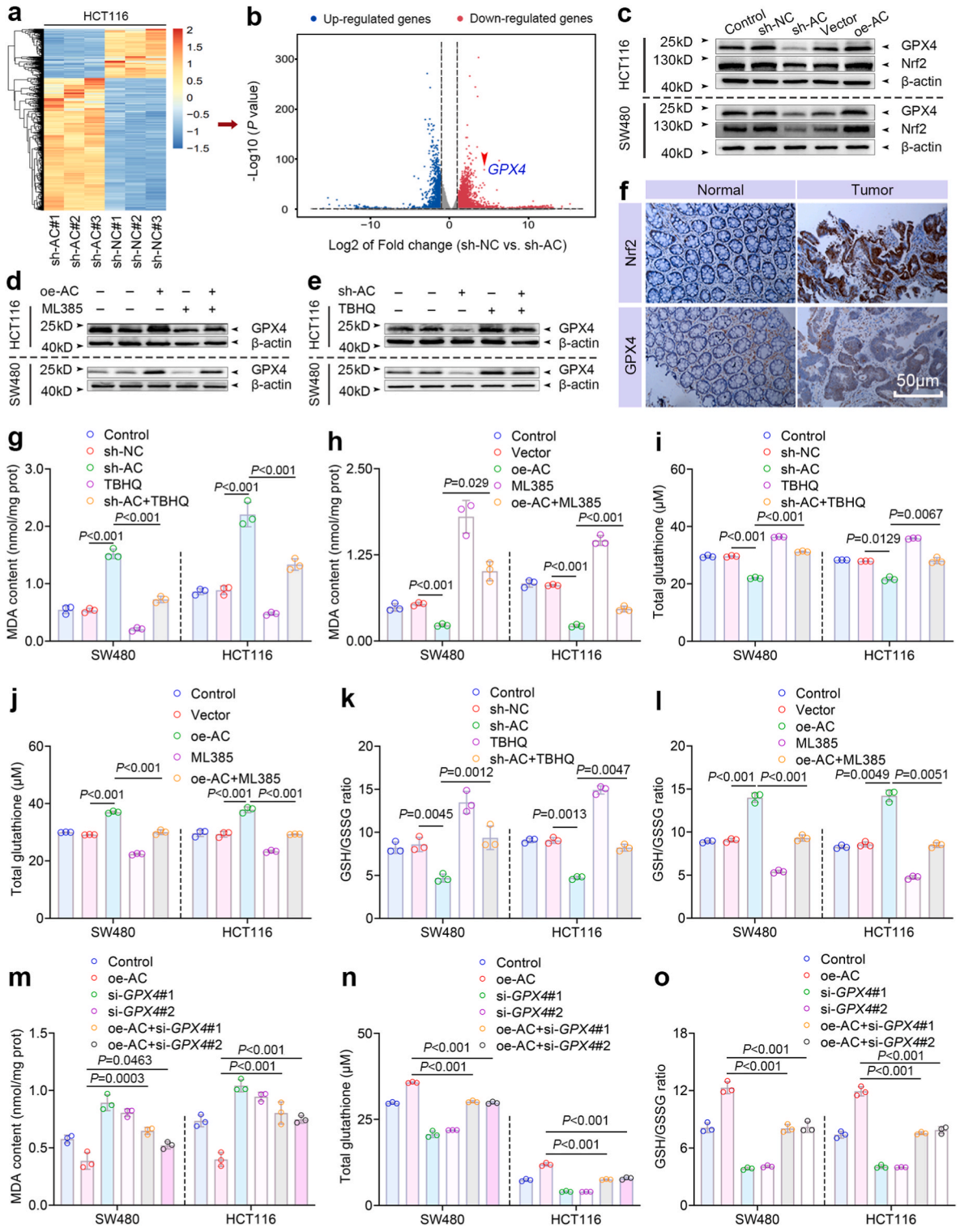

Fig. 5. AC145207.5 impedes CRC cell ferroptosis through the Nrf2/GPX4 signaling pathway. (**a**) Heatmap of RNA-Seq data illustrating the differentially expressed genes (DEGs) in HCT116 cells following AC145207.5 knockdown. (**b**) Volcano plot displaying the DEGs between three paired negative control and sh-AC groups in HCT116 cells, with a significant decrease in *GPX4* expression observed in AC145207.5-knockdown cells. (**c**) Western blotting analysis of Nrf2 and GPX4 protein levels after AC145207.5 interference in both HCT116 and SW480 cells. (**f**) IHC analysis of Nrf2 and GPX4 expression in paired CRC and adjacent normal tissues. (**d and e**) Rescue experiments assessing GPX4 expression in HCT116 and SW480 cells treated with AC145207.5 overexpression and ML385 (10 μM; pretreate for 1 h) or AC145207.5 knockdown and TBHQ (20 μM; pretreate for 12 h) by Western blotting. (**g and h**) Rescue experiments measuring MDA levels in HCT116 and SW480 cells treated with AC145207.5 overexpression and ML385 or AC145207.5 knockdown and TBHQ. (**i-l**) Rescue experiments determining total glutathione levels and the GSH/GSSG ratio in HCT116 and SW480 cells treated with AC145207.5 overexpression and ML385 or AC145207.5 knockdown and TBHQ. (**m**) Rescue experiments quantifying MDA levels in HCT116 and SW480 cells treated with AC145207.5 overexpression and *GPX4* knockdown. (**n and o**) Rescue experiments evaluating total GSH levels and the GSH/GSSG ratio in HCT116 and SW480 cells treated with AC145207.5 overexpression and *GPX4* knockdown. Statistical analyses were performed using the one-way ANOVA.

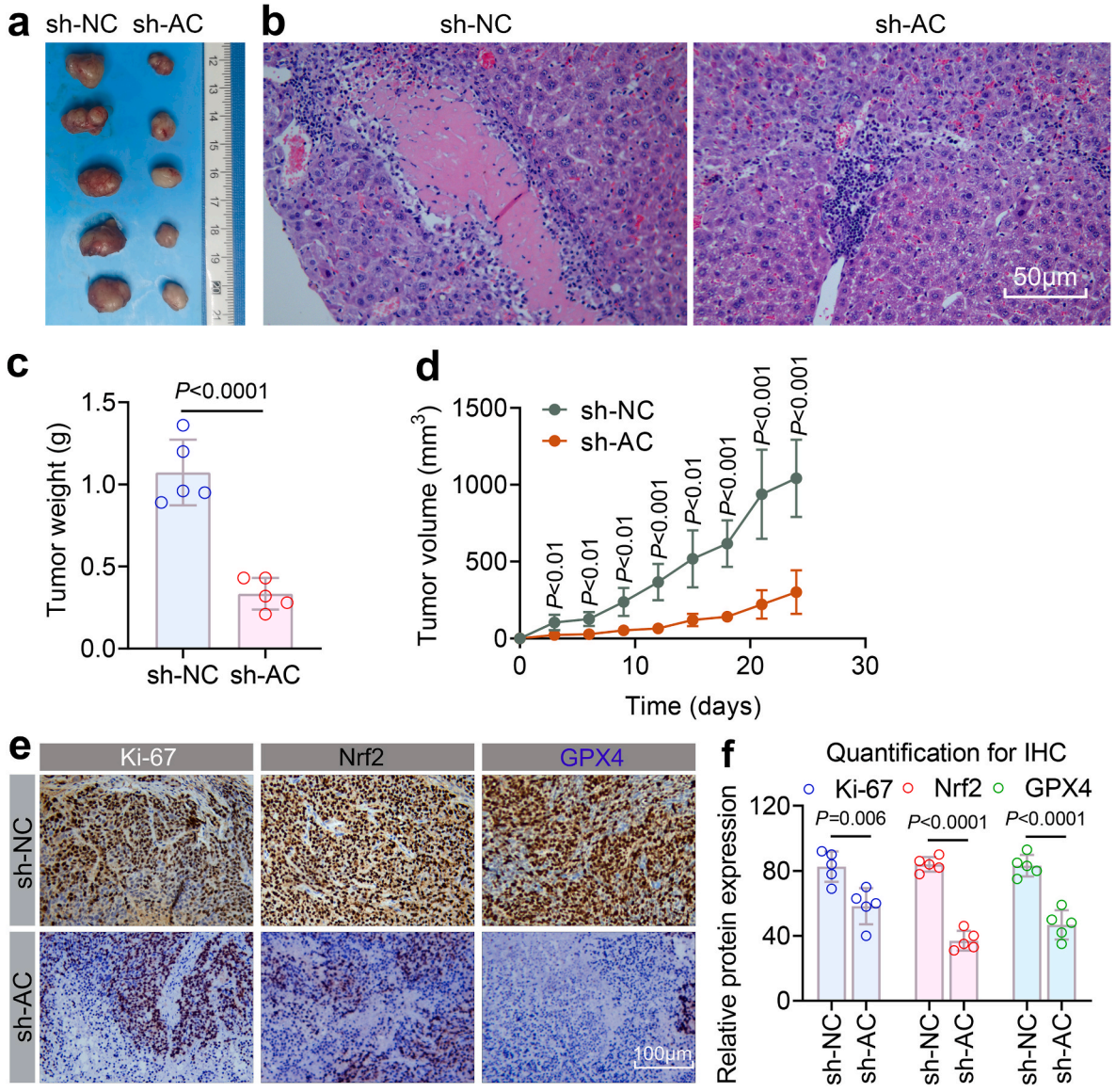

Fig. 6. AC145207.5 promotes CRC tumorigenesis *in vivo*. (**a**) Images of subcutaneous tumors in BALB/c nude mice injected with HCT116 cells treated with sh-NC and sh-AC. (**b**) H&E staining was applied to identify the subcutaneous tumors. (**c**) Tumor weights of the subcutaneous xenografts. Statistical analyses were performed using the Student's *t*-test. (**d**) Tumor growth curves are shown after subcutaneous injection of HCT116 cells containing stably silenced AC145207.5 or negative control. Statistical analyses were performed using the two-way ANOVA. (**e and f**) Representative IHC images of CRC showing Ki-67, GPX4, and Nrf2 staining, along with corresponding quantification of Ki-67, GPX4, and Nrf2 levels in CRC. Statistical analyses were performed using the Student's *t*-test.

ferroptosis [31]. Additionally, activation of the Wnt/β-catenin/TCF4 pathway has been associated with the upregulation of GPX4 expression, subsequently impeding ferroptosis in gastric cancer cells [32]. Validating the role of GPX4 in AC145207.5-mediated ferroptosis regulation, qPCR and Western blotting analyses confirmed the positive regulation of GPX4 expression by AC145207.5.

Moreover, depletion of *GPX4* levels in CRC cells exhibiting high AC145207.5 expression led to a reversal of the AC145207.5-induced tumor proliferation and ferroptosis phenotype, suggesting that AC145207.5 inhibits ferroptosis by upregulating GPX4. The *Nrf2* gene, known to modulate GPX4 expression and regulate ferroptosis [33,34], was found to influence the increased GPX4 expression induced by AC145207.5 upregulation. This was demonstrated by the attenuation of GPX4 expression with the Nrf2 inhibitor ML385 and its restoration with the Nrf2 activator TBHQ. Our study posits that Nrf2 serves as a crucial modulator of oxidative stress, significantly influencing ferroptotic pathways. Initial data suggest that AC145207.5 may enhance Nrf2 activity, thereby augmenting the cellular antioxidant response and potentially offering protection against ferroptosis. However, if oxidative stress levels exceed the compensatory capacity of Nrf2, ferroptosis may occur. This duality highlights the complexity of Nrf2's role in ferroptosis, and we intend to further elucidate this relationship in our ongoing research. These findings establish a novel link between AC145207.5 and the upregulation of GPX4 through the activation of Nrf2 during the occurrence and progression of CRC.

5. Conclusion

Our groundbreaking investigation unveils, for the first time, the notable elevation of AC145207.5 within CRC tissues, highlighting its pivotal role in driving tumor proliferation and progression. Our observations reveal a novel interaction between HNRNPC and AC145207.5, facilitated by m6A modification, leading to the heightened expression of AC145207.5. This surge in AC145207.5 levels instigates and propels the onset of CRC progression through a ferroptosis-dependent mechanism. Furthermore, silencing AC145207.5 significantly diminishes *GPX4*

expression by orchestrating Nrf2 activity, triggering a cascade of ferroptotic events characterized by redox dysregulation and peroxidative injury, ultimately dictating the fate of CRC cells (Fig. 7). These revelatory findings underscore the potential of HNRNPC/AC145207.5/Nrf2/GPX4 axis as valuable diagnostic markers and therapeutic targets in CRC management.

CRediT authorship contribution statement

Dan Liu: Writing – review & editing, Writing – original draft, Supervision, Funding acquisition. **Shanshan Lin:** Methodology, Investigation, Formal analysis, Data curation. **Yueben Hu:** Software, Resources, Methodology, Data curation. **Jianyong Xiong:** Validation, Resources, Project administration. **Hongtao Wan:** Methodology, Investigation, Data curation, Conceptualization. **Yanglin Chen:** Resources, Project administration, Methodology, Investigation. **Taohui Ding:** Validation, Methodology, Investigation, Conceptualization. **Hu Zhao:** Visualization, Validation, Project administration. **Renjie Jiang:** Project administration, Methodology, Investigation, Formal analysis. **Zhijiang Huang:** Methodology, Investigation. **Dengke Yao:** Investigation. **Ming Li:** Formal analysis, Data curation. **Xiaojian Zhu:** Writing – review & editing, Writing – original draft. **Bo Yi:** Writing – review &

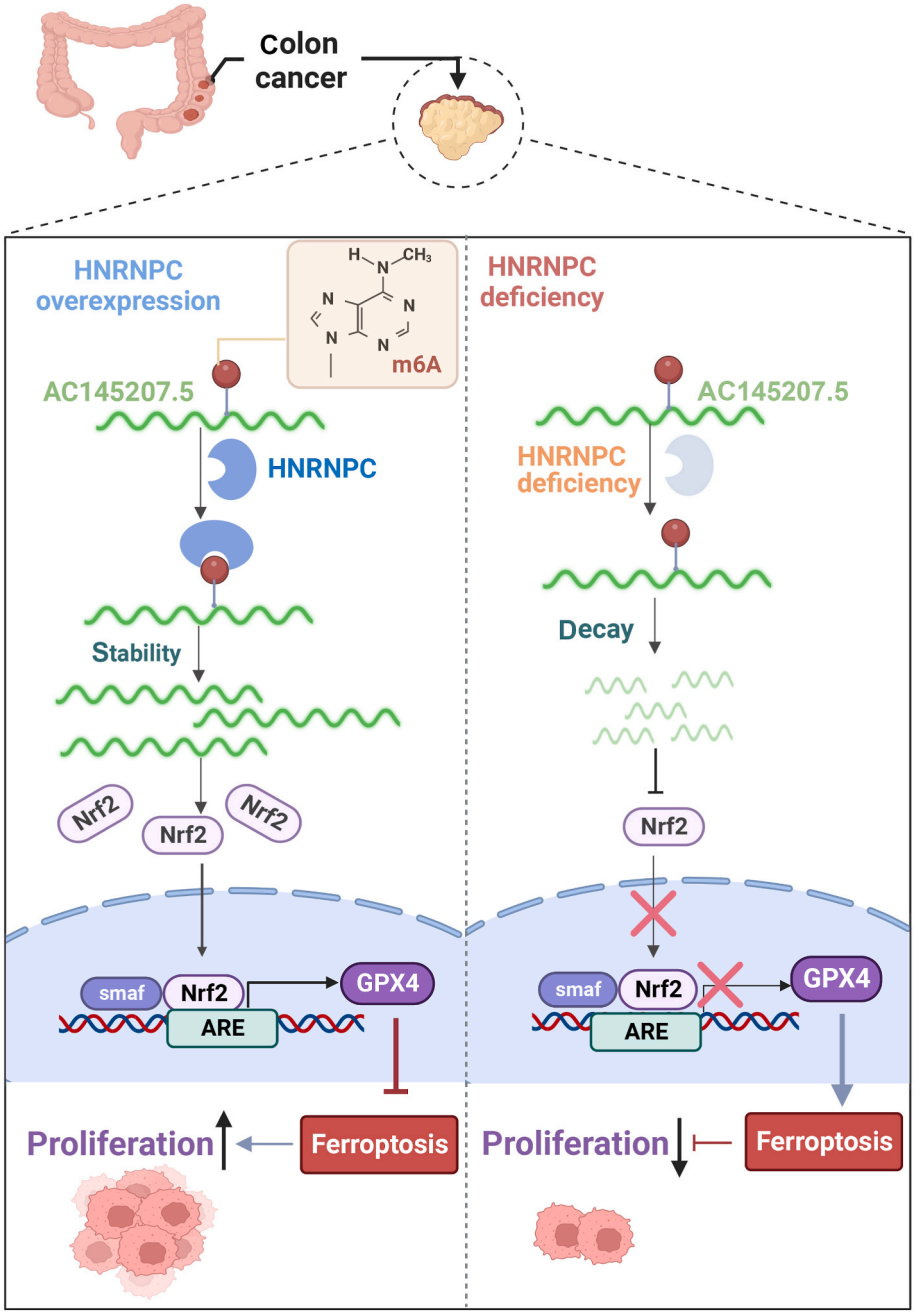

Fig. 7. Graphical abstract of the role of m6A-modified AC145207.5 stabilized by HRRNPC in promoting tumorigenesis in CRC by regulating ferroptosis through the Nrf2/GPX4 axis. The m6A reader HNRNPC is proposed to directly recognize and bind the specific m6A motif of AC145207.5, thereby promoting its stability and expression (Left). Increased AC145207.5 activates the transcription factor Nrf2, enabling it to enter the nucleus and promote *GPX4* transcription, subsequently inhibiting ferroptosis and enhancing the proliferation of CRC cells. Conversely, defective *HNRNPC* expression leads to rapid decay of AC145207.5 due to the loss of its stabilizing effect (Right). Decreased levels of AC145207.5 fail to activate the Nrf2 signaling pathway, resulting in Nrf2's inability to enter the nucleus and inhibiting *GPX4* transcription. Consequently, ferroptosis is triggered, and the proliferation of CRC cells is impeded.

editing, Visualization, Validation, Funding acquisition.

Ethics approval and consent to participate

Prior to commencement, the research protocol underwent rigorous scrutiny and garnered approval from the Ethics Review Committee of Nanchang Medical College. Informed consent was diligently obtained from all participating patients. The ethical conduct of all animal experimentation adhered strictly to the principles delineated in the Guide for the Care and Use of Laboratory Animals by International Committees. Every conceivable measure was taken to curtail the quantity of animals utilized and alleviate any potential distress or discomfort experienced by the subjects.

Availability of data and materials

The datasets generated and/or analyzed during the current study are available from the article and supplementary information.

Funding

This study was supported by grants from the National Natural Science Foundation of China (*No*.81760731, *No*.81760587), the Jiangxi province Health Commission (*No*.202310886), Excellent Young Scientists Fund of Jiangxi Cancer Hospital (*No*.2021EYS01), Jiangxi Provincial Natural Science Foundation (*No*.20202BABL206093), Technology Plan Project of Jiangxi Provincial Health Commission (*No*.202310875) and Gastrointestinal Tumors Diagnosis, Treatment, and Drug Resistance Research Team of Nanchang Medical College (*No*.NYTD202209).

Declaration of competing interest

The authors declare that there are no conflicts of interest related to this research. No financial or personal relationships with other people or organizations that could inappropriately influence or bias the work are disclosed.

Acknowledgements

We would like to express our gratitude to the Department of Pathology at Jiangxi Cancer Hospital for their valuable assistance in performing immunohistochemical staining of CRC tissues for this study.

Appendix A. Supplementary data

Supplementary data to this article can be found online at https://doi.org/10.1016/j.ncrna.2025.04.002.

Abbreviations

CRC	Colorectal Cancer
LncRNA	Long non-coding RNA
HNRNPC	Heterogeneous Nuclear Ribonucleoprotein C
TCGA	The Cancer Genome Atlas
GEO	Gene Expression Omnibus
ROC	Receiver Operating Characteristic
AUC	Area Under the Curve
m6A	N^6-adenosine methylation
FBS	Fetal Bovine Serum
shRNA	Short Hairpin RNA
PVDF	Polyvinylidene Difluoride
ROS	Reactive Oxygen Species
MDA	Malondialdehyde
GSH	Glutathione
GSSG	Glutathiol
TBA	Thiobarbituric Acid
FISH	Fluorescence iIn Situ Hybridization
RT-qPCR	Real-time Quantitative polymerase chain reaction
RIP	RNAImmunoprecipitation
Me-RIP	Methylated RNA Immunoprecipitation
RBPs	RNA-Binding Proteins
OD	Optical Density
GO	Gene Ontology
KEGG	Kyoto Encyclopedia of Genes and Genomes
Fer-1	Ferrostatin-1
TBHQ	Tert-Butylhydroquinone
H&E	Hematoxylin and Eosin
IHC	Immunohistochemistry

References

[1] S.G. Patel, J.J. Karlitz, T. Yen, C.H. Lieu, C.R. Boland, The rising tide of early-onset colorectal cancer: a comprehensive review of epidemiology, clinical features, biology, risk factors, prevention, and early detection, Lancet Gastroenterol. Hepatol. 7 (3) (2022) 262–274.
[2] R.L. Siegel, N.S. Wagle, A. Cercek, R.A. Smith, A. Jemal, Colorectal cancer statistics, 2023, CA Cancer J. Clin. 73 (3) (2023) 233–254.
[3] T. Nojima, N.J. Proudfoot, Mechanisms of lncRNA biogenesis as revealed by nascent transcriptomics, Nat. Rev. Mol. Cell Biol. 23 (6) (2022) 389–406.
[4] X. Lin, S. Zhuang, X. Chen, J. Du, L. Zhong, J. Ding, et al., lncRNA ITGB8-AS1 functions as a ceRNA to promote colorectal cancer growth and migration through integrin-mediated focal adhesion signaling, Mol. Ther. 30 (2) (2022) 688–702.
[5] S. Zhao, B. Guan, Y. Mi, D. Shi, P. Wei, Y. Gu, et al., LncRNA MIR17HG promotes colorectal cancer liver metastasis by mediating a glycolysis-associated positive feedback circuit, Oncogene 40 (28) (2021) 4709–4724.
[6] L. Chang, J. Ding, J. Pu, J. Zhu, X. Zhou, Q. Luo, et al., A novel lncRNA LOC101928222 promotes colorectal cancer angiogenesis by stabilizing HMGCS2 mRNA and increasing cholesterol synthesis, J. Exp. Clin. Cancer Res. 43 (1) (2024) 185.
[7] J. Pan, F. Liu, X. Xiao, R. Xu, L. Dai, M. Zhu, et al., METTL3 promotes colorectal carcinoma progression by regulating the m6A-CRB3-Hippo axis, J. Exp. Clin. Cancer Res. 41 (1) (2022) 19.
[8] Y. Bao, J. Zhai, H. Chen, C.C. Wong, C. Liang, Y. Ding, et al., Targeting m(6)A reader YTHDF1 augments antitumour immunity and boosts anti-PD-1 efficacy in colorectal cancer, Gut 72 (8) (2023) 1497–1509.
[9] A. Xia, W. Yuan, Q. Wang, J. Xu, Y. Gu, L. Zhang, et al., The cancer-testis lncRNA lnc-CTHCC promotes hepatocellular carcinogenesis by binding hnRNP K and activating YAP1 transcription, Nat. Cancer 3 (2) (2022) 203–218.
[10] Y. Cai, T. Lyu, H. Li, C. Liu, K. Xie, L. Xu, et al., LncRNA CEBPA-DT promotes liver cancer metastasis through DDR2/β-catenin activation via interacting with hnRNPC, J. Exp. Clin. Cancer Res. 41 (1) (2022) 335.
[11] X.J. Luo, Y.X. Lu, Y. Wang, R. Huang, J. Liu, Y. Jin, et al., m6A-modified lncRNA FAM83H-AS1 promotes colorectal cancer progression through PTBP1, Cancer Lett. (2024) 217085.
[12] Y. Bian, S. Xu, Z. Gao, J. Ding, C. Li, Z. Cui, et al., m(6)A modification of lncRNA ABHD11-AS1 promotes colorectal cancer progression and inhibits ferroptosis through TRIM21/IGF2BP2/FOXM1 positive feedback loop, Cancer Lett. 596 (2024) 217004.
[13] Q. Xue, D. Yan, X. Chen, X. Li, R. Kang, D.J. Klionsky, et al., Copper-dependent autophagic degradation of GPX4 drives ferroptosis, Autophagy 19 (7) (2023) 1982–1996.
[14] G. Lei, L. Zhuang, B. Gan, Targeting ferroptosis as a vulnerability in cancer, Nat. Rev. Cancer 22 (7) (2022) 381–396.
[15] B. Hassannia, P. Vandenabeele, B.T. Vanden, Targeting ferroptosis to iron out cancer, Cancer Cell 35 (6) (2019) 830–849.
[16] H. Yang, Y. Hu, M. Weng, X. Liu, P. Wan, Y. Hu, et al., Hypoxia inducible lncRNA-CBSLR modulates ferroptosis through m6A-YTHDF2-dependent modulation of CBS in gastric cancer, J. Adv. Res. 37 (2022) 91–106.
[17] R. Zhang, T. Pan, Y. Xiang, M. Zhang, H. Xie, Z. Liang, et al., Curcumenol triggered ferroptosis in lung cancer cells via lncRNA H19/miR-19b-3p/FTH1 axis, Bioact. Mater. 13 (2022) 23–36.
[18] D. Pe'Er, S. Ogawa, O. Elhanani, L. Keren, T.G. Oliver, D. Wedge, Tumor heterogeneity, Cancer Cell 39 (8) (2021) 1015–1017.
[19] J.L. Reading, D.R. Caswell, C. Swanton, Tumor heterogeneity impairs immunogenicity in mismatch repair deficient tumors, Nat. Genet. 55 (10) (2023) 1610–1612.
[20] Z. Wu, X. Zuo, W. Zhang, Y. Li, R. Gui, J. Leng, et al., m6A-Modified circTET2 interacting with HNRNPC regulates fatty acid oxidation to promote the proliferation of chronic lymphocytic leukemia, Adv. Sci. 10 (34) (2023) e2304895.
[21] Y.T. Tan, J.F. Lin, T. Li, J.J. Li, R.H. Xu, H.Q. Ju, LncRNA-mediated posttranslational modifications and reprogramming of energy metabolism in cancer, Cancer Commun. 41 (2) (2021) 109–120.
[22] W. Huang, H. Li, Q. Yu, W. Xiao, D.O. Wang, LncRNA-mediated DNA methylation: an emerging mechanism in cancer and beyond, J. Exp. Clin. Cancer Res. 41 (1) (2022) 100.
[23] E.M. McCabe, T.P. Rasmussen, lncRNA involvement in cancer stem cell function and epithelial-mesenchymal transitions, Semin. Cancer Biol. 75 (2021) 38–48.

[24] Z. Zheng, X. Zeng, Y. Zhu, M. Leng, Z. Zhang, Q. Wang, et al., CircPPAP2B controls metastasis of clear cell renal cell carcinoma via HNRNPC-dependent alternative splicing and targeting the miR-182-5p/CYP1B1 axis, Mol. Cancer 23 (1) (2024) 4.
[25] L. Yang, T. WenTao, Z. ZhiYuan, L. Qi, L. YuXiang, Z. Peng, et al., Cullin-9/p53 mediates HNRNPC degradation to inhibit erastin-induced ferroptosis and is blocked by MDM2 inhibition in colorectal cancer, Oncogene 41 (23) (2022) 3210–3221.
[26] D. Liu, X. Luo, M. Xie, T. Zhang, X. Chen, B. Zhang, et al., HNRNPC downregulation inhibits IL-6/STAT3-mediated HCC metastasis by decreasing HIF1A expression, Cancer Sci. 113 (10) (2022) 3347–3361.
[27] B. Lian, S. Yan, J. Li, Z. Bai, J. Li, HNRNPC promotes collagen fiber alignment and immune evasion in breast cancer via activation of the VIRMA-mediated TFAP2A/DDR1 axis, Mol. Med. 29 (1) (2023) 103.
[28] H. Yan, R. Talty, C.H. Johnson, Targeting ferroptosis to treat colorectal cancer, Trends Cell Biol. 33 (3) (2023) 185–188.
[29] S. Zhang, S. Gou, Q. Zhang, X. Yong, B. Gan, D. Jia, FSP1 oxidizes NADPH to suppress ferroptosis, Cell Res. 33 (12) (2023) 967–970.
[30] Y. Liu, Y. Wan, Y. Jiang, L. Zhang, W. Cheng, GPX4: the hub of lipid oxidation, ferroptosis, disease and treatment, Biochim. Biophys. Acta Rev. Cancer 1878 (3) (2023) 188890.
[31] G. Wang, S. Qin, L. Chen, H. Geng, Y. Zheng, C. Xia, et al., Butyrate dictates ferroptosis sensitivity through FFAR2-mTOR signaling, Cell Death Dis. 14 (4) (2023) 292.
[32] Y. Wang, L. Zheng, W. Shang, Z. Yang, T. Li, F. Liu, et al., Wnt/beta-catenin signaling confers ferroptosis resistance by targeting GPX4 in gastric cancer, Cell Death Differ. 29 (11) (2022) 2190–2202.
[33] Y. Wang, S. Yan, X. Liu, F. Deng, P. Wang, L. Yang, et al., PRMT4 promotes ferroptosis to aggravate doxorubicin-induced cardiomyopathy via inhibition of the Nrf2/GPX4 pathway, Cell Death Differ. 29 (10) (2022) 1982–1995.
[34] X. Liu, C. Yan, C. Chang, F. Meng, W. Shen, S. Wang, et al., FOXA2 suppression by TRIM36 exerts anti-tumor role in colorectal cancer via inducing NRF2/GPX4-regulated ferroptosis, Adv. Sci. 10 (35) (2023) e2304521.